Proceedings of the ASME Turbo Expo 2022
Turbomachinery Technical Conference and Exposition
GT2022
June 13-17, 2022, Rotterdam, The Netherlands

GT2022-83201

DEVELOPMENT AND EVALUATION OF SHAPED FILM COOLING HOLES DESIGNED FOR ADDITIVE MANUFACTURING

Michael T. Furgeson[1,*], Emma M. Veley[2], Christopher Yoon[1], Daniel Gutierrez[1], David G. Bogard[1], Karen A.Thole[2]

[1]The University of Texas at Austin
Austin, TX
[2]Pennsylvania State University
State College, PA

ABSTRACT

Film cooling remains a critical technology for cooling gas turbine components. In recent years, additive manufacturing (AM) has been used to develop novel film cooling hole designs which significantly increase the film cooling effectiveness. However, engine scale AM builds have imperfections and roughness that can have a noticeable effect on performance. In this study, 9-9-3 shaped film cooling holes were constructed at engine scale using metal AM, specifically direct laser metal sintering (DMLS). These "as built" geometries were characterized through computerized tomography (CT) scans to quantify deviations from holes with design intent, or "as-designed" holes. To evaluate the performance of the "as-built" holes compared to "as-designed" holes, both adiabatic and overall cooling effectiveness were measured experimentally for 5x scale models. The larger scale enabled the use of finite deposition modeling (FDM) to construct hole geometry that closely matched the "as-designed" holes and the CT scans of the "as-built" holes. Two versions of the 9-9-3 hole were studied, the 9-9-3 rounded inlet (RI) hole with rounding at the inlet, and the 9-9-3 rounded inlet and exit (RIE) hole with additional rounding at the hole inlet, and rounding at the hole exit. Results showed that the adiabatic effectiveness and overall cooling effectiveness for the "as-built" holes were similar to the performance of the "as-designed" film cooling holes for both hole geometries tested.

Keywords: Additive Manufacturing, Film Cooling

NOMENCLATURE

A_c	cross-sectional area [mm^2]
D	hole diameter [m]
k	thermal conductivity [W/m-K]
L	hole length [m]
l	length coordinate along hole axis
$\dot{m}$	mass flow rate [g/s]
N	sample size
P	hole pitch [m]
R_a	arithmetic mean roughness [μm]
RI	Rounded Inlet
RIE	Rounded Inlet and Exit
t	wall thickness
T	temperature [K]
U	velocity [m/s]
z	surface height [mm]

Greek letters

α	injection angle [°]
δ	uncertainty
η	adiabatic effectiveness
μ	mean surface height
ϕ	overall effectiveness
ρ	density [kg/m^3]
χ	coolant warming factor

Dimensionless groups

Bi	Biot number
DR	density ratio
I	momentum flux ratio
M	blowing ratio
Nu	Nusselt number
Pr	Prandtl number
Re	Reynolds number
VR	velocity ratio

Superscripts and subscripts

∞	freestream
b	bias
c	coolant
DI	design intent
f	fluid
j	jet

*Corresponding author: mfurges@utexas.edu

h hydraulic diameter
o orifice
p precision
r repeatability
s solid
v Venturi
x flat plate coordinate

1. INTRODUCTION

In modern gas turbine engines, extensive cooling of turbine components in the hot section is critical as temperatures can reach up to 1600-1800 °C [1, 2]. An important component of this cooling is film cooling, where relatively cool air from the compressor is routed downstream and ejected through holes in the blades and vanes of the hot section. This ejected coolant creates a thin "film" across the surface, thus maintaining safe material operating temperatures. While the technology has been around for more than half a century, there have been significant changes in recent decades. The development of shaped holes, such as the 7-7-7 shaped hole by Schroeder et al. [3], resulted in improved cooling performance over cylindrical holes [4, 5]. The primary difference between conventional shaped holes and cylindrical holes is the presence of a diffusing outlet, where 7-7-7 refers to the two lateral and forward expansion angles [3], respectively. It is also common to refer to the forward expansion as “laid back”, and the lateral expansion as “fan shaped” [5]. This diffusion reduces jet separation, and thus produces better coolant jet adhesion to the blade/vane surface.

Although traditional shaped holes are manufacturable using electron discharge machining (EDM) [6, 7], recent studies have investigated holes made possible only by using additive manufacturing. This includes holes with rounded inlets [8] as well as novel adjoint optimized holes [9]. Evidence has shown that a rounded hole inlet, in contrast to a traditional “sharp” inlet, offers significant improvement to performance [8]. This considered, the design for the baseline case for this study was a nominally 9-9-3 rounded inlet hole, or RI hole.

Addtively manufacturing film cooling holes presents unique challenges, notably when using powder bed fusion (PBF) techniques such as direct metal laser sintering (DMLS). DMLS often produces significant roughness in cooling holes which can distort flow and reduce cooling performance as shown by Stimpson et al [6] and Vinton et al. [10]. Examining holes manufactured using DMLS reveals that the majority of this roughness occurs near sharp corners, and that deformations in this region often result in noticeable deviation from design intent. In an effort to resolve this, another hole design used in this study incorporated additional rounding of the inlet as well as rounding of the diffuser exit, and these holes were referred to as rounded inlet and exit holes (RIE). Schematics of the RI and RIE holes can be seen in Fig. 1, where both holes have an injection angle, $\alpha = 30°$. Note that the schematics show the radius of curvature for the inlet rounding of the RI hole was $R = 0.25D$, and the inlet and exit rounding for the RIE hole was $R = 0.4D$ and $R = 0.2D$, respectively. When examining the figure, note that the holes are described as “nominally" 9-9-3, as unforeseen errors in preparing the geometry resulted in irregularities in diffuser shape. Therefore, the true forward and lateral expansion angles are 2.8° and 8.6°, respectively. The upstream side of the diffuser is also tilted forward 2.2°.

To make quantitative comparisons, the adiabatic, or film effectiveness is used to measure the cooling performance of film jets. This effectiveness is defined by [2]

$$\eta = \frac{T_\infty - T_{aw}}{T_\infty - T_c} \tag{1}$$

where T_∞ is the mainstream temperature, T_{aw} is the adiabatic wall temperature, and T_c is the coolant temperature at exit of the film cooling hole. Using the adiabatic wall temperature isolates the effect of film cooling. To examine the effects of combined internal and film cooling, the overall cooling effectiveness ϕ is used [11]

$$\phi = \frac{T_\infty - T_w}{T_\infty - T_c} \tag{2}$$

where T_w is the temperature of the conducting wall, and T_c is the internal channel coolant temperature. Using the overall effectiveness becomes especially useful when considering the surface roughness of additively manufactured holes. This roughness has been shown to improve internal channel and bore cooling [6, 7] by acting in a similar fashion to rib turbulators [12]. Note that overall effectiveness as a representation of heat transfer augmentation due to internal cooling is described by Dyson et al. [11]. In that study, the following relationship for 1-D conduction through the wall was derived

$$\phi = \frac{1 - \chi\eta}{1 + Bi + \frac{h_\infty}{h_c}} + \chi\eta \tag{3}$$

where χ is the coolant warming factor, Bi is the Biot number, and h_∞/h_c is the ratio of external to internal heat transfer coefficient (HTC). From this relationship it is clear that correct use of the overall effectiveness requires matching engine conditions, notably for the parameters Bi, h_∞/h_c, and η. Although most engine conditions are proprietary, Dyson et al. [11] estimate an engine matched Biot number of $0.1 < Bi < 1$, and Mclintic et al. [13] report a $Bi = 0.8$. Using nominal values from Bunker [14], a reasonable estimate of HTC ratio is $h_\infty/h_c \approx 2.5$. Note that χ was not explicitly determined in this study as Equation 2, rather

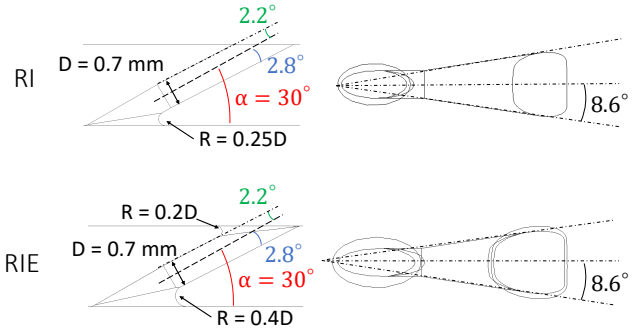

FIGURE 1: ENGINE SCALE SCHEMATIC OF THE 9-9-3 RI AND RIE

than Equation 3 was used to find experimental ϕ. Bi may be found using the equation [15]

$$Bi = \frac{h_\infty t}{k_s} \tag{4}$$

where t is the wall thickness, and k_s is the thermal conductivity of the solid. Heat transfer coefficients for the external and internal surface may be found using Nusselt number correlations. The external heat transfer coefficient is determined using the following relationship for a flat plate with constant heat flux and turbulent flow [15]

$$Nu_x = \frac{h_\infty x}{k_f} = 0.0308 Re_x^{4/5} Pr^{1/3} \tag{5}$$

where Re is the Reynolds number, Pr is the Prandtl number, subscript f denotes the fluid, and subscript x denotes the location on the flat plate. For this study, Nu_x was determined using the wall coordinate location x of the film cooling holes. Note that Equation 5 is valid when evaluating the flat-plate facility used in this study, but it is not valid when evaluating a turbine airofil. The internal heat transfer coefficient is found using the Dittus-Boelter equation for heated, fully developed turbulent channel flow [15].

$$Nu_{D_h} = \frac{h_c D_h}{k_f} = 0.0243 Re_{D_h}^{4/5} Pr^{0.4} \tag{6}$$

where D_h is the hydraulic diameter of the internal channel.

There are three primary scaling parameters used in film cooling. These are the velocity ratio VR, blowing ratio M, and momentum flux ratio I [2]. For this study the focus will be on VR, as it has been shown to be the optimal scaling parameter with varying density ratio DR [16, 17]. The velocity ratio and density ratio are defined as follows

$$VR = \frac{V_j}{V_\infty} \tag{7}$$

$$DR = \frac{\rho_j}{\rho_\infty} \tag{8}$$

where V is the velocity, ρ is the density, and subscript j denotes the film jet (specifically at the exit of the hole). Internal channel inlet velocity ratio VR_c is also considered. VR_c is found using the relationship

$$VR = \frac{V_c}{V_\infty} \tag{9}$$

where V_c is defined at inlet of the coolant channel.

With this understanding, the study presented experimentally evaluates two film cooling holes at approximately 5x engine scale. These include the 9-9-3 RI and RIE holes, evaluated using both the adiabatic effectiveness and overall cooling effectiveness with internal channel co-flow conditions. Additionally, each of these cases were evaluated with "as-designed" (AD) and "as-built" (AB) geometry. As-designed holes maintain the designed geometry in Fig. 1, and as-built holes capture the deformities and inherent roughness of metal AM. In total this results in eight different base coupons that were tested, which provided sufficient data for a thorough understanding of the behavior of the RI and RIE holes. To accurately resolve the as-built conditions produced by metal AM, both the RI and RIE hole were constructed using DMLS at approximately engine scale. The resulting "as-built" geometry was then CT scanned, such that a 5x scale version could be printed using a fused deposition modeling (FDM) printer.

2. CHARACTERIZATION OF AS-BUILT GEOMETRIES

An EOS-M280 powder bed fusion printer at Penn State University was used to manufacture two coupons based on the large-scale studies. Each coupon had five cooling holes that were either of RI or RIE design. One of the five holes for each design was scaled up and tested experimentally in this study, although it should be recognized that there is some variation between each hole. During manufacture using the EOS-M280, the axis of the hole metering section was oriented with the build direction (vertical), seen in Fig 2, as this orientation produces the least distortion from the design intent [18]. A combination of solid, box, and conical support structures were used to hold the parts to the substrate during the build process. The supports were removed after the build was annealed to remove residual stresses. The coupons were made using Inconel 718 with 40 μm layers. Pictures of the as-built hole exits can be seen in Fig 3, with a painted external surface. The machine parameters, shown in Table 1, were consistent between geometries.

An industrial computed tomography (CT) scanner was used to reconstruct a three-dimensional nondestructive representation of each as-built hole. With a scanning resolution of 20 μm (voxel size), the software's adaptive surface determination can ascertain the surface at 1/10th the voxel size [19]. Once the as-built surfaces of the coupons were deduced, these were directly compared to the design intent.

Local deviations from the design intent for both cooling holes are shown in Fig 4. Positive values of deviation indicate

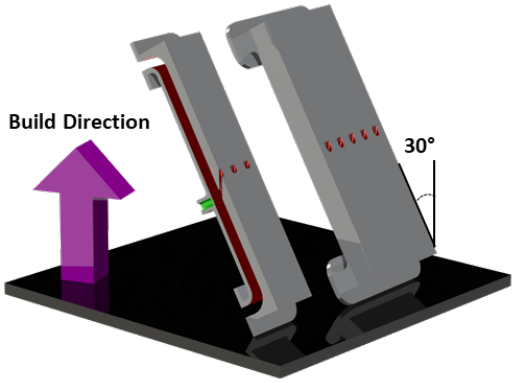

FIGURE 2: BUILD ORIENTATION OF COUPON WITH A CROSS SECTION SHOWING THE COOLING HOLE ORIENTATION

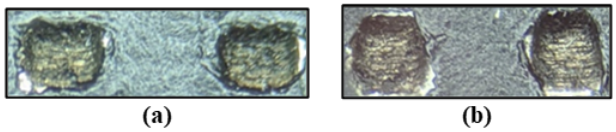

FIGURE 3: PHOTOS OF THE AS-BUILT HOLE EXITS FOR THE (A) RI AND (B) RIE HOLES.

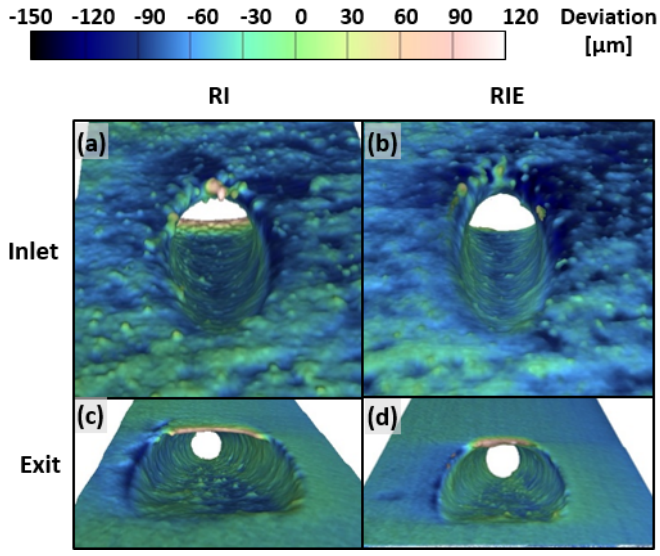

FIGURE 4: LOCAL DEVIATION FROM DESIGN INTENT AT THE (A&B) INLET AND (C&D) EXIT OF (A&C) RI AND (B&D) RIE.

material where no material was intended based on the design. Negative values indicate that there is no material where material was intended. The local deviations are mostly negative suggesting that the holes are oversized relative to the design intent. Cross-sectional slices of the CT scanned surface along the meter axis, such as those shown in Fig. 5 and 6, were used to calculate the cross-sectional area and perimeter of the holes. This cross sectional area was normalized against design intent and included in Table 2, along with other hole parameters. Note that the values shown in this table are average values determined by measuring all five holes which were manufactured, such that variability is considered. The ± ranges presented for cross sectional area and hydraulic diameter represent variation across the five holes from the average. The table shows that although both designs are oversized, the metering section of RIE is closer to the design intent. Both holes show a tendency to build poorly along the downward facing region of the inlet fillet, seen at $l/L = 0.32$ in Fig. 5 and 6. Note here that l is the length coordinate, and L is the overall hole length. Also note that outlet rounding for the RIE impacts the cross section at $l/L = 0.86$. Surface roughness as a result of poor build is known to have an impact on flow through channels [18]. The arithmetic mean roughness is found using the relation

TABLE 1: DMLS PROCESS PARAMETERS

Parameter	Value
Material	Inconel 718
Layer thickness	0.04 mm
Material setting	Performance IN718 04 211
Material scaling X	0.124%
Material Scaling Y	0.124%
Beam Offset	0.115 mm

$$R_a = \frac{1}{N}\sum_{i=1}^{N}|z_i - \mu| \tag{10}$$

where N is sample size, z is the surface height, and μ is the mean surface height. The arithmic mean roughness is a measure of the magnitude of the average distance between the surface and mean fitted surface. For the as-built geometries a plane was fitted to the laidback surface of the diffuser and a cylinder was fit to the metering section of each hole resulting in a Gaussian distribution. The average Ra between the meter and diffuser sections was within the 1/10th voxel size uncertainty. The resulting average Ra of the RIE is approximately twice that of the RI. Fig. 7 shows example traces along the laidback surface of the holes. The variations in roughness feature sizes can be seen across these 1 mm traces.

Another geometric scale important to effectiveness is the wall thickness, t. The wall separates the coolant flow from the mainstream flow and the thickness of the wall is proportional to the conduction through the wall which in turn affects effectiveness.

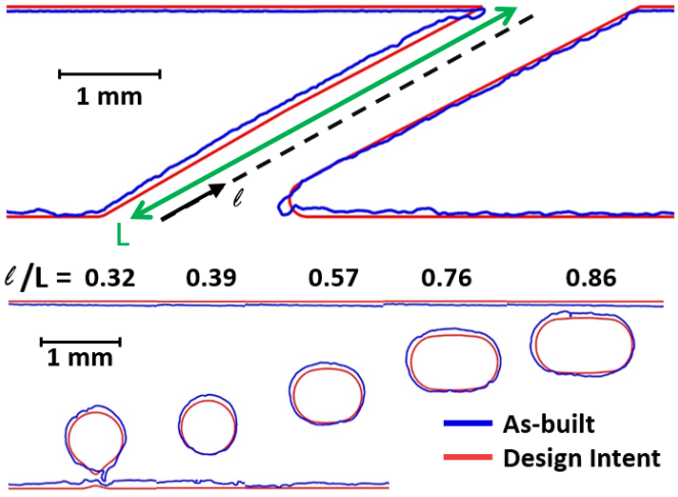

FIGURE 5: CROSS-SECTIONS OF THE RI AS-BUILT AND DESIGN INTENT SURFACES.

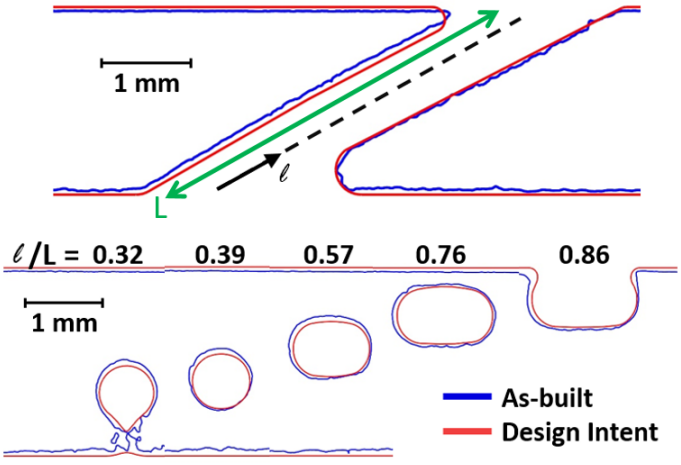

FIGURE 6: CROSS-SECTIONS OF THE RIE AS-BUILT AND DESIGN INTENT SURFACES.

The design intent wall thickness for this study was $t_{DI} = 3D$. The average wall thicknesses of both AB coupons were within 4% of the design intent (2.0955 mm). The as-built values are reported in Table 2, with standard deviations of 13 μm. Further detail of this characterization process may be found in [20].

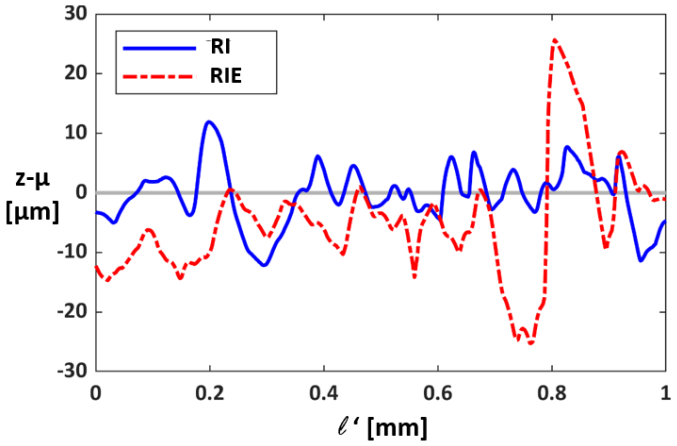

FIGURE 7: TRACES OF ROUGHNESS HEIGHT ON THE LAIDBACK SURFACES

TABLE 2: HOLE SPECIFICATIONS AND PARAMETERS

Hole	$\frac{D_h}{D_{h,DI}}$	$\frac{A_c}{A_{c,DI}}$	$\frac{t}{t_{DI}}$	R_a $[\mu m]$
RI	1.09 ± 0.04	1.21 ± 0.01	0.987	6.5
RIE	1.04 ± 0.05	1.13 ± 0.02	0.983	12.7

3. EXPERIMENTAL METHODOLOGY

Experimental tests were performed for the 9-9-3 RI and RIE coupons over a range of velocity ratios. These experiments were run with a co-flow internal channel, in an effort to be comparable to previous results found by testing metal AM holes at Penn State University [6, 7].

3.1 Wind Tunnel Facility and Test Section

The experiments were performed in the low-speed, recirculating wind tunnel at the University of Texas at Austin, which was used for many past studies such as [8, 13, 16, 21]. A diagram of the wind tunnel is shown in Fig. 8, where it can be seen that there is a primary “mainstream" flow loop and secondary “coolant" flow loop. Note the operating pressure for the wind tunnel facility is close to atmospheric pressure, and that both flow loops are dried using desiccant to prevent frosting. The primary flow loop is held at a constant temperature of 295K using chilled water in conjunction with a PID controller. Before entering the test section, mainstream flow is conditioned by passing through a series of honeycomb and screens, and then a nearly isotropic turbulent flow is generated using a turbulence grid. In this study, the turbulence intensity in the test section was 3.8%. The secondary flow loop supplies coolant to the coolant channel and film cooling holes. The coolant is air cooled by liquid nitrogen to 246K to satisfy a density ratio $DR = 1.2$. Coolant density was found from the perfect gas law using measurements of temperature at the coolant channel inlet and mainstream. In this study, DR may be found using the coolant inlet temperature as there is minimal coolant warming with smooth wall geometry. For this same reason, note that T_c was measured at the coolant channel inlet for both adiabatic effectiveness and overall cooling effectiveness.

Coolant mass flow rate is measured both upstream and downstream of the test section using an orifice and Venturi flow meter, respectively. The resulting mass flow deficit between the two flow meters may be used in calculating hole VR. The orifice meter was calibrated using a laminar flow element, and the Venturi meter was calibrated directly against the upstream orifice meter to minimize bias. Coolant flowrate was controlled by adjusting upstream and downstream valves limiting coolant supply and exhaust. More information on the details of this tunnel can be found in Anderson et al. [22] and Wilkes et al. [21]. Since those works were published, the most significant change has been to the test section, which was redesigned to produce co-flow rather than cross-flow (see Fig. 9).

As shown in Fig. 9, modular design of the test section allowed the authors to swap between different film cooling hole coupons and adjacent surfaces. For experiments measuring adiabatic effectiveness, the surface material was closed cell polyurethane foam with a thermal conductivity of $k \approx 0.03$ W/m·K. For overall cooling effectiveness measurements, the surface material was DuPont Corian with $k \approx 1.0$ W/m·K. Corian’s thermal conductivity produced an engine matched Biot number of $Bi = 0.89$ with the conditions described in §§3.3. Surface temperature measurements were made using an infrared camera (FLIR A655sc), which was calibrated *in-situ* with surface thermocouples. To ensure consistent and optimal emissivity of the surface, all components in the measurement area were painted black. Laterally averaged effectiveness was monitored live for all VR to ensure steady state conditions were reached. Multiple thermocouples and pressure taps were installed at the inlet and exit of the channel to monitor coolant temperature and pressure.

3.2 Manufacture of Test Coupons

Hole coupons were manufactured at the UT facility at nominally 5x engine scale using a fused deposition modeling (FDM) printer. The printer used was a Prusa MK3 printer, which operates using g-code produced by Slic3r based software. Each coupon was printed with the mainstream facing surface flush to the print bed. Adiabatic coupons were printed using polylactic acid (PLA) filament at 15% infill. Jones et al. [8] estimate the thermal conductivity of these coupons to be $k \approx 0.14$ W/m-K. Coupons used for overall effectiveness measurements were printed using a conductive nylon filament (TC Poly Ice 9 Rigid [23]) with thermal conductivity of $k \approx 1$ W/m-K in the build direction (“through-plane”) and $k \approx 4$ W/m-K "in-plane". As with Corian, the nylon filament was used as its through-plane thermal conductivity produces an engine matched Biot number of $Bi = 0.89$. Note that following manufacturer guidelines [23], the nylon filament required an elevated extrusion temperature of 290°C. Furthermore, a borosilicate glass print surface and glue were implemented to reduce print warping resulting from using 100% infill.

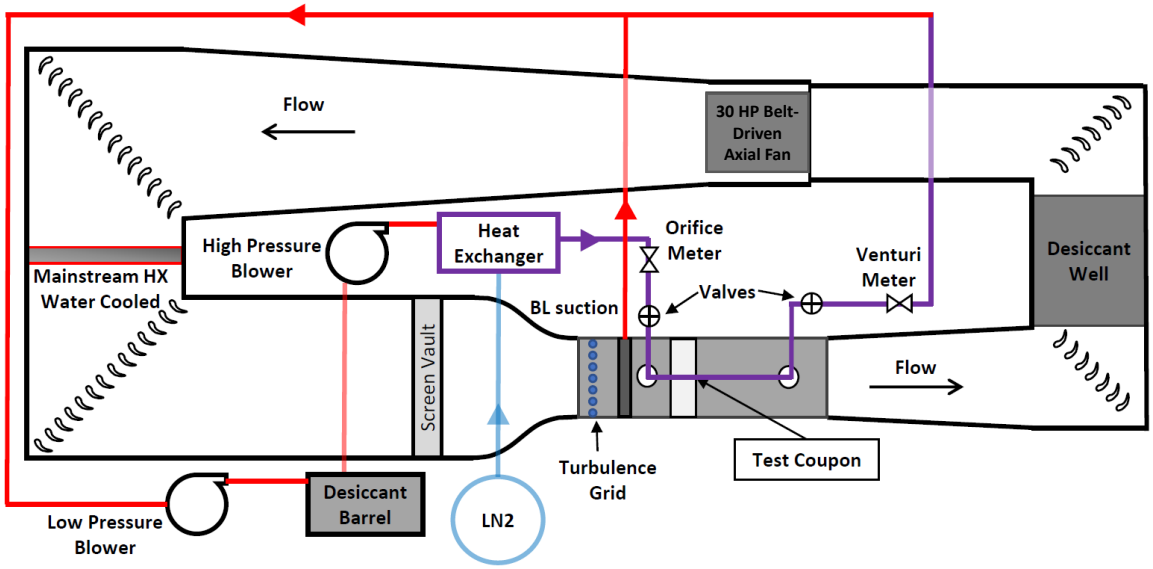

FIGURE 8: DIAGRAM OF WIND TUNNEL FACILITY USED FOR THE STUDY

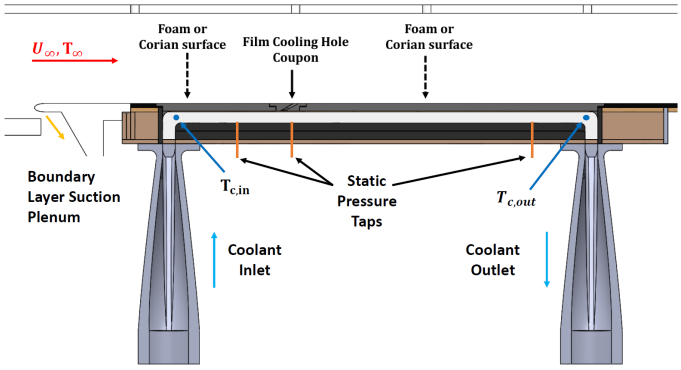

FIGURE 9: SCHEMATIC OF THE TEST SECTION

All coupons were printed using a nozzle diameter of 0.4 mm, and the majority of coupons were printed using a "standard" layer height of 0.2 mm. The standard layer height is critical to the conducting coupons to ensure the correct thermal conductivity. Note that using a layer height of 0.2 mm produces some roughness in the AD coupons, and results in some loss of resolution for the AB coupons. To evaluate the impact of using the standard layer height, adiabatic RI coupons were also constructed using a "fine" layer height of 0.05 mm. Experimental results comparing the performance of these coupons are presented in §4.

Images of the hole outlets and inlets of all coupons experimentally tested in this study are presented in Fig. 10. It may be seen in the images that roughness features are reflected in all AB holes. These features were included using computerized tomography (CT) scans of one hole for each geometry characterized in §2. However, there is a noticeable difference between both the AD and AB coupons printed with standard and fine layer height. These considerations will again be discussed further in §4. To validate the internal hole structure of the standard FDM coupons, midplane mockups were created and compared directly to the CT scans in Fig. 11. Major defects at the inlets and outlets of the holes are circled in both the CT scans and the resulting FDM coupons. Also included in the figure are images of the as-designed holes for comparison. When examining the RIE AD image, it should be noted that some of the paint used for contrast unintentionally bled over the outlet rounding feature.

3.3 Experimental Setup and Conditions

Two hole designs were tested: the RI and RIE. For each hole design, an as-designed (AD) version and as-built (AB) version were tested using both an adiabatic and conducting wall. Furthermore, adiabatic versions of the RI AD and RI AB hole constructed with fine layer height were tested, and the results were compared to results with standard layer height. All of these cases are presented in Table 3. Note that because tests for adiabatic effectiveness do not use a perfectly insulating wall, the following 1-D conduction correction was applied for these cases

$$\eta_{corrected} = \frac{\eta_{measured} - \eta_0}{1 - \eta_0} \tag{11}$$

where $\eta_0 = 0.078$ was determined by experimentally measuring surface temperature using a blank coupon with no film cooling. Experimental conditions used in this study are presented in Table 4. With the exception of DR, non-dimensional parameters listed are engine matched. For all experiments, density ratio and channel inlet velocity ratio were held constant at $DR = 1.2$ and $VR_c = 0.2$, respectively. Note the density ratio is defined at the exit of the film cooling hole and calculated using the perfect gas law. It may be observed that engine matched parameters of Bi and h_∞/h_c were maintained for overall effectiveness experiments, following the nominal guidelines described in §1. η is matched by using the same hole geometry and matching hole Reynolds number Re_D.

3.4 Repeatability and Uncertainty

The mean bias and precision uncertainties for some experimental parameters are reported in Table 5. Instrumenta-

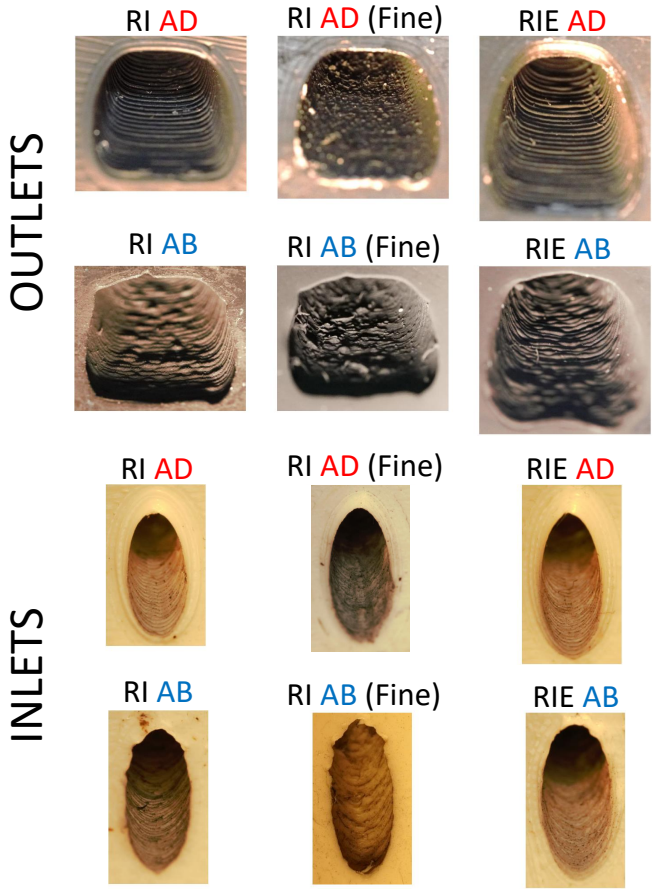

FIGURE 10: HOLE OUTLETS AND INLETS OF COUPONS

TABLE 3: EXPERIMENTAL CASES

Case	Design	Type	Material	Build
1	RI	AD	Adiabatic	Standard
2	RI	AD	Conducting	Standard
3	RI	AB	Adiabatic	Standard
4	RI	AB	Conducting	Standard
5	RIE	AD	Adiabatic	Standard
6	RIE	AD	Conducting	Standard
7	RIE	AB	Adiabatic	Standard
8	RIE	AB	Conducting	Standard
9	RI	AD	Adiabatic	Fine
10	RI	AB	Adiabatic	Fine

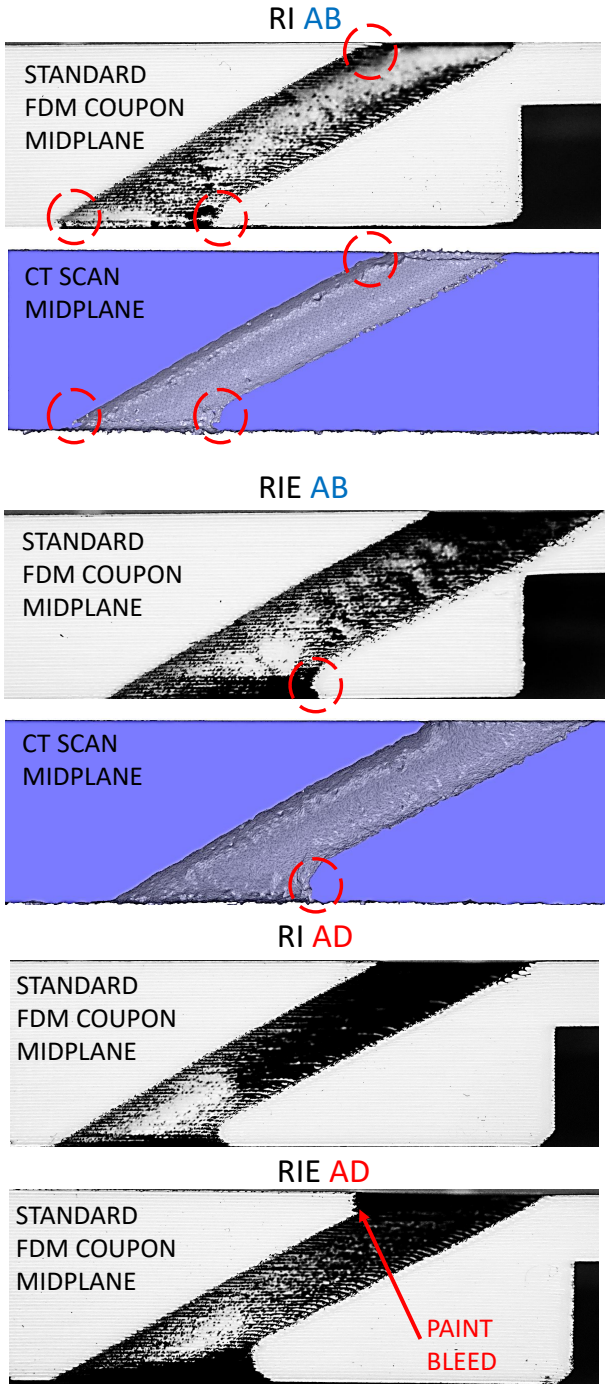

FIGURE 11: HOLE MIDPLANE COMPARISON OF COUPONS

tion uncertainties were determined using the statistical methods desribed by Figliola & Beasley [24] and Montgomery & Runger [25]. Uncertainties for calculated parameters were found using the sequential perturbation methods described by Moffat [26]. Repeatability was quantified for the fine RI AD coupon using test-to-test repeatability of the parameter $\bar{\eta}$ over an interval of 16 days. For $VR = 1.67$, test-to-test repeatability was determined to be $\delta_R(\bar{\eta}) = \pm 0.02$. The two curves are in Fig. 12, along with the curve of in-test repeatability. Test-to-test repeatability for all recorded VR is presented in the area averaged plot also shown.

4. RESULTS

Experimental results for all cases are presented in this section. It should be understood that as presented in Table 2, the hole areas of the as-built holes are different that that of the as-designed holes. This was a result of deformities produced during DMLS manufacturing. Therefore, equivalent diameters were determined for the AB builds using the minimum cross sectional areas provided in Table 2. Using these diameters ensures that non-dimensional parameters are accurately represented.

TABLE 4: EXPERIMENTAL CONDITIONS

Parameter	Value	Units
Mainstream Velocity, U_∞	24.9	m/s
Mainstream Temperature, T_∞	295	K
Coolant Temperature, T_c	246	K
Design Hole Diameter, D	3.8	mm
Reynolds Number, Re_D	6200	[-]
Turbulence Intensity, Tu_∞	3.8	%
Boundary Layer Thickness, δ_{99}/D	2.5	[-]
Wall Thickness, t	11.4	[mm]
Biot Number, Bi (Corian surface)	0.89	[-]
HTC Ratio, h_∞/h_c (Corian surface)	2.5	[-]
Coolant Channel Height, H_c/D	3.4	[-]
Density Ratio, DR	1.20	[-]
Coolant Jet Velocity Ratio, VR	0.35 - 3.33	[-]
Channel Inlet Velocity Ratio, VR_c	0.20	[-]

TABLE 5: MEAN BIAS AND PRECISION UNCERTAINTY

Parameter	$\pm\delta_p$	$\pm\delta_b$	Units
Mainstream Velocity, U_∞	0.1	0.01	m/s
Mainstream Temperature, T_∞	0.01	0.1	K
Coolant Temperature, T_c	0.1	0.1	K
Upstream Mass Flow Rate, $\dot{m}_o$	0.03	0.2	g/s
Downstream Mass Flow Rate, $\dot{m}_v$	0.04	0.2	g/s
Density Ratio, DR	0.0002	0.0007	[-]
Velocity Ratio, VR	0.01	0.07	[-]
Channel Inlet Velocity Ratio, VR_c	0.001	0.002	[-]
Overall Effectiveness, ϕ	0.001	0.02	[-]
Adiabatic Effectiveness, η	0.002	0.02	[-]

For the RI-AB hole, this corrected diameter is 4.18 mm, while for the RIE-AB hole, it is 4.04 mm. This results in ratios of as-built to designed diameters of $(D_{AB}/D_{AD})_{RI} = 1.10$ and $(D_{AB}/D_{AD})_{RIE} = 1.06$, respectively. Note that as this was realized during experimentation, the range of VR for the RI-AB geometries differs slightly from that of the other geometries. These cases were run assuming the designed diameter, and a correction to VR was applied using the equivalent diameter in post-processing.

In Fig. 13, area averaged effectiveness 5-30D downstream for all experimental cases is shown, and data for a 7-7-7 sharp inlet hole is presented for comparison. It may be observed that all rounded inlet 9-9-3 hole geometries outperform the standard 7-7-7 hole. Furthermore, trends of performance are repeatable in both the adiabatic and matched Biot number coupons. While not the primary focus of this study, it may be observed that the RIE-AD hole and RI-AD hole perform similarly. This would suggest that additional rounding at the inlet and exit of the hole does not effect performance for the designed geometry.

Although there appears to be some difference between the AD and AB holes in Fig. 13, there is also variation in P/D. The

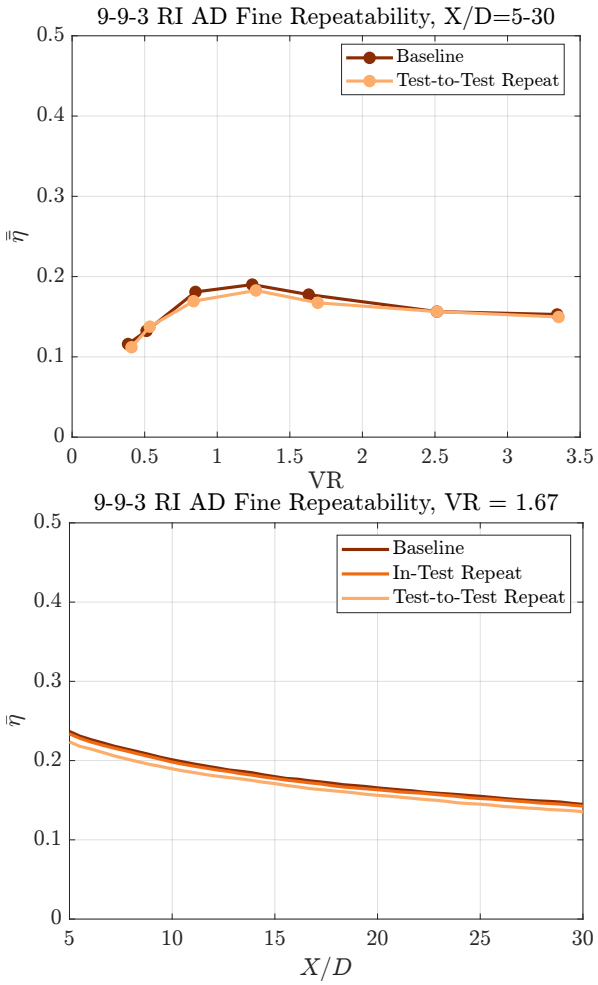

FIGURE 12: REPEATABILITY OF EXPERIMENTAL MEASUREMENTS

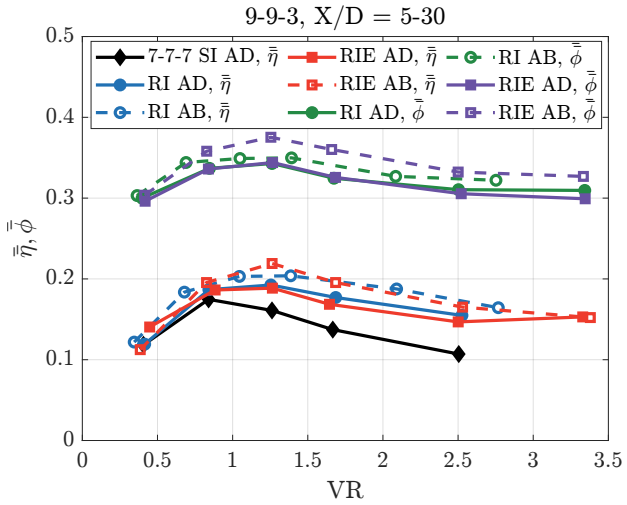

FIGURE 13: AREA AVERAGED ADIABATIC AND OVERALL COOLING EFFECTIVENESS OVER X/D = 5 to 30

pitch is the same for all cases, but as noted previously, equivalent diameter varies as a result of the DMLS build process. Consequently, for the RI AB hole, $P/D = 5.61$, and for the RIE AB hole, $P/D = 5.77$. To compare these results with those of the RI

and RIE AD holes, which had $P/D = 6$, adjustments to η values were made to determine the equivalent $\bar{\bar{\eta}}$ for the AB holes for $P/D = 6.0$. The superposition technique for these adjustments is described by Bogard & Thole [2]. Following this superposition, $\bar{\bar{\eta}}$ values were re-plotted in Fig. 14. Note that $\bar{\bar{\phi}}$ is not adjusted as the same superposition technique may not be used for overall effectiveness. In Fig. 14, it may be seen that the performances of the AB and AD geometries are similar, and do not differ outside of the bounds of uncertainty presented in Table 5. Furthermore, the performances of the RI and RIE AB geometries are also similar.

Additional insights may be made by examining the contours of η in Fig. 15-16 and of ϕ in Fig. 17-18. Note that wall putty was applied at the seam between the test coupon and the test surface, which creates a thin visible band at $X/D \approx 3$. This band is caused by both the declined emmissivity of the wall putty in comparison to the black paint, and the increased thermal conductivity of the material in comparison to polyurethane foam. Also note that because the hole diameter varies between the AD and AB cases, the scales of X/D and Z/D in the figures differ over the same measurement area.

Examining the adiabatic effectiveness contours in Fig. 15-16, jet spreading is significant at $VR \approx 0.42$, but the coolant quickly mixes with the mainstream flow and provides minimal cooling far downstream. At $VR \approx 2.50$, the jet narrows significantly, but cools more effectively at the centerline farther downstream. Although not shown for brevity, the peak performing case of $VR \approx 1.25$ provides balance between these two ends of the spectrum. Performance remains high farther downstream, but sufficient jet spreading is maintained. Furthermore, asymmetries and gaps in the jet profile are shown for the AB holes. This is likely caused by the deformities described in §2, but does not appear to significantly effect $\bar{\bar{\eta}}$ as shown in Fig. 14. Note that although there are asymmetries, jet-to-jet uniformity is good among all adiabatic cases. Although not traditionally seen in DMLS manufactured geometry, this uniformity is present in this study as only one hole was CT scanned for each geometry (RI and RIE). This same hole geometry was used for every hole in the AB coupons.

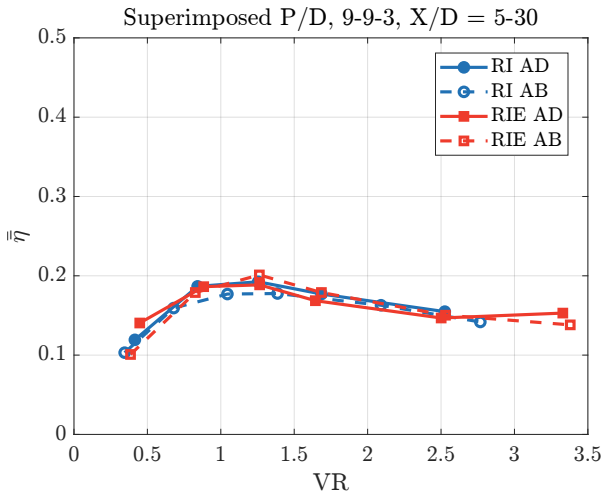

FIGURE 14: AREA AVERAGED ADIABATIC EFFECTIVENESS OVER X/D = 5 to 30 WITH ADJUSTED P/D

Examining the overall effectiveness contours in Fig. 17-18, insights may also be made about bore cooling. As expected in a conducting model, there is variation in temperature at the exit of the hole diffuser between the case of $VR \approx 0.42$ and $VR \approx 2.50$. This may be stated as this region is in view of the IR camera. As more coolant is ejected through the hole at higher velocity, internal hole convection increases. Comparing the near hole region of the AB holes to the AD holes in Fig. 18, bore cooling is more significant for the AB holes. The distinction of bore cooling, rather than film cooling is used here as ϕ upstream and to the sides of the jet is greater. This region can only be impacted by internal channel and bore cooling effects, and as the coolant channel inlet VR_c is the same among all cases, internal channel cooling upstream of the hole is the same. When examining Fig. 18, also note that there is some hole-to-hole non-uniformity in the jet profile. This may be caused by some artificial hole deformation as a result of FDM printing with nylon, which is a challenging resin to print with. However, at the lower velocity ratio case in Fig. 17, hole-to-hole uniformity is good.

To further examine the effects of bore cooling in the conducting model, laterally averaged overall cooling effectiveness was plotted for the RIE coupon at $VR = 0.42$ and $VR = 2.50$ in Fig. 19. In the figure, it may be observed that the peaks of the AB holes are higher than that of the AD holes. However, it must again be considered that P/D differs between the AB and AD geometries. In turn, this comparison is difficult to make, notably downstream of the film cooling hole. Still, it may be seen that there is as much as a 10% increase in $\bar{\phi}$ in the case of $VR = 2.50$ for $X/D = -2$ to $X/D = 0$. This significant increase in $\bar{\phi}$ inside the hole may be attributed to increased bore cooling, likely due to rougher walls for the AB case. This increased bore cooling would also augment $\bar{\phi}$ a short distance downstream of the hole.

As discussed in §§3.2, additional adiabatic RI coupons were constructed with the FDM printer using a "fine" layer height of 0.05 mm, in contrast to the coupons constructed with a "standard" layer height of 0.2 mm. This was an effort to evaluate the effect of layer height on the performance of those coupons. Following completion of these experiments, the results were plotted alongside the standard layer height results in Fig. 20, noting that AB $\bar{\bar{\eta}}$ values were adjusted to their equivalent value at $P/D = 6$ as in Fig. 14. This was done so accurate comparison can be made between the AD and AB geometry. It may be observed in the figure that the AD coupons perform similarly at both layer heights. This suggests that results found using the standard layer height AD coupons accurately reflect the performance of holes with design intent. However, Fig. 20 also shows a decline in performance for the fine RI AB coupon in comparison to the standard RI AB. This difference is significant and should be evaluated. Insight may also be made by examining Fig. 21 and 22, which display $\bar{\eta}$ and η contours, respectively. In Fig. 21, it may be seen that the standard layer height coupon is better performing than the fine layer height coupon for a significant length downstream. However, the difference between the two curves does decline with increasing X/D. In Fig. 22, it may be observed that the jet profile appears narrower and there is reduced coverage in the fine layer height case.

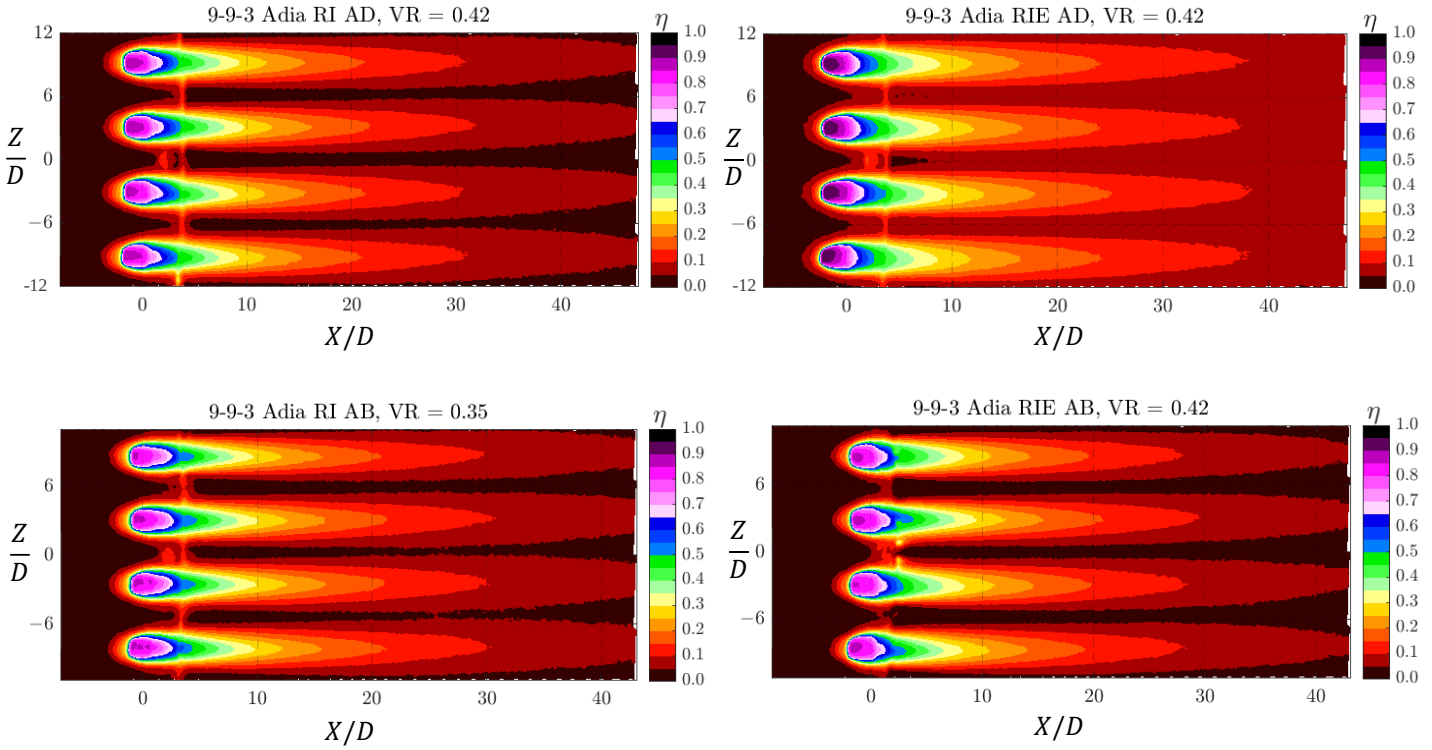

FIGURE 15: ADIABATIC EFFECTIVENESS CONTOURS AT VR = 0.42

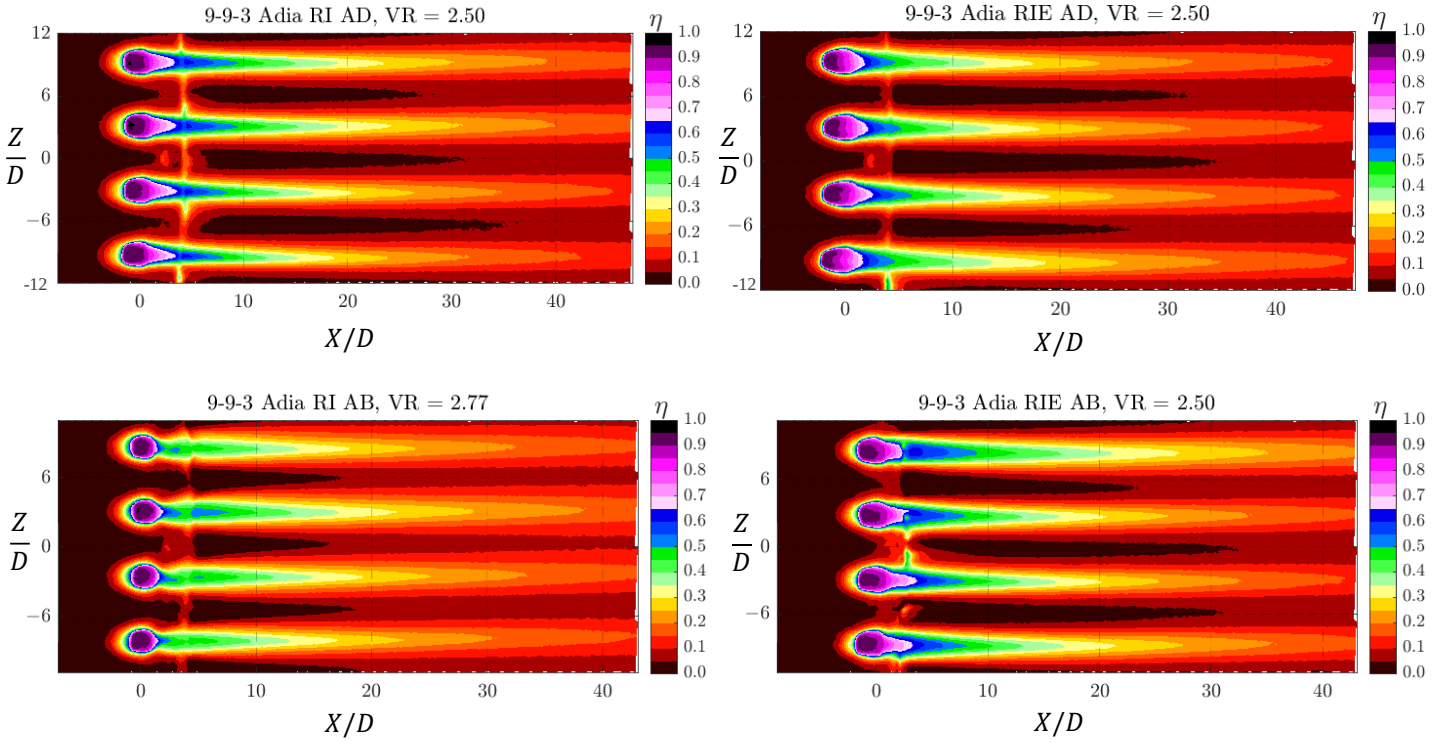

FIGURE 16: ADIABATIC EFFECTIVENESS CONTOURS AT VR = 2.50

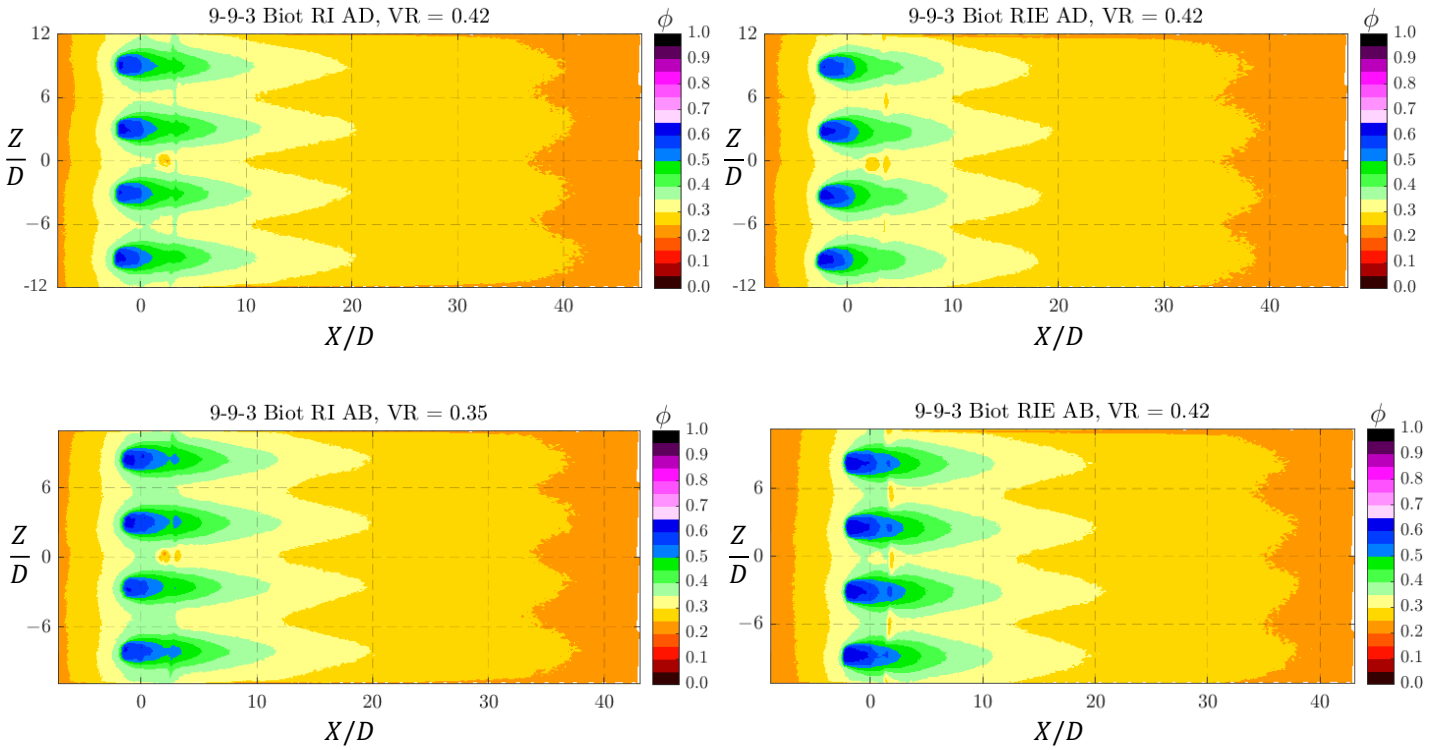

FIGURE 17: OVERALL COOLING EFFECTIVENESS CONTOURS AT VR = 0.42

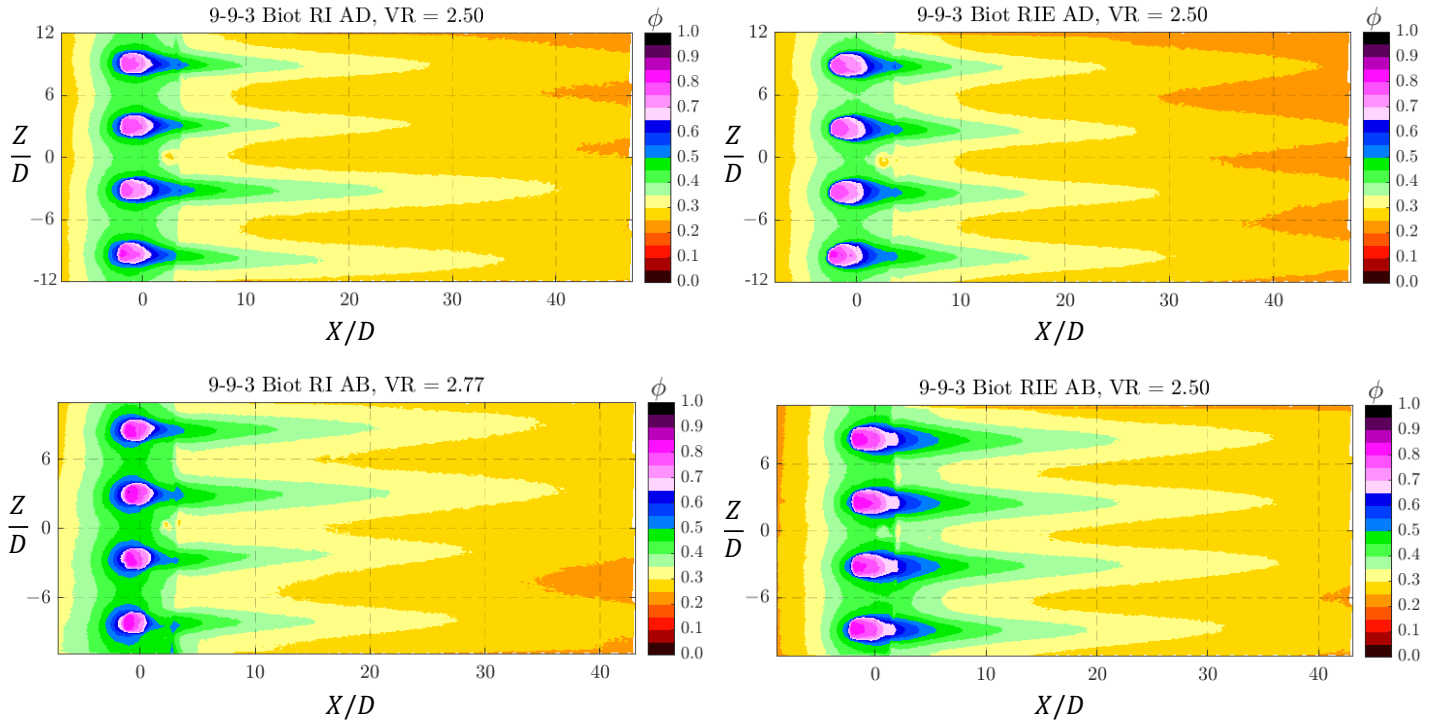

FIGURE 18: OVERALL COOLING EFFECTIVENESS CONTOURS AT VR = 2.50

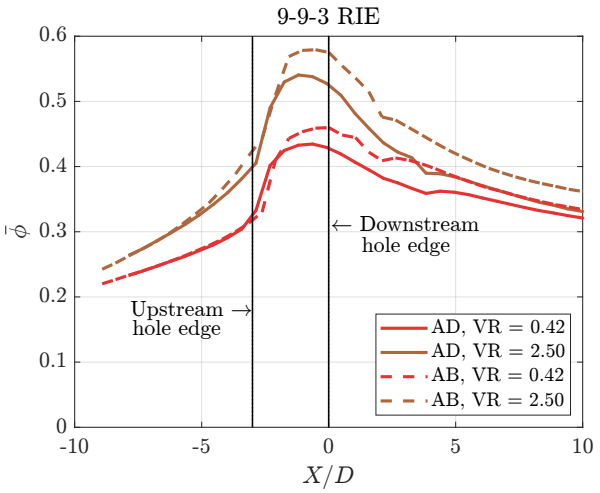

FIGURE 19: NEAR HOLE LATERALLY AVERAGED ϕ CURVES FOR THE 9-9-3 RIE AT VR=0.42 AND VR=2.50.

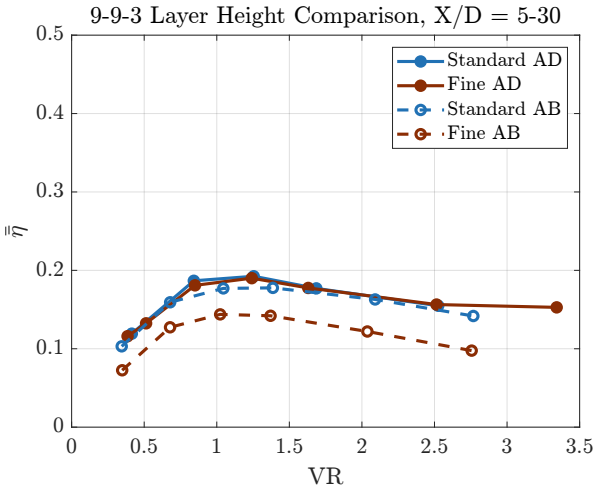

FIGURE 20: AREA AVERAGED η OVER X/D = 5 to 30 FOR THE 9-9-3 RI USING STANDARD AND FINE BUILDS

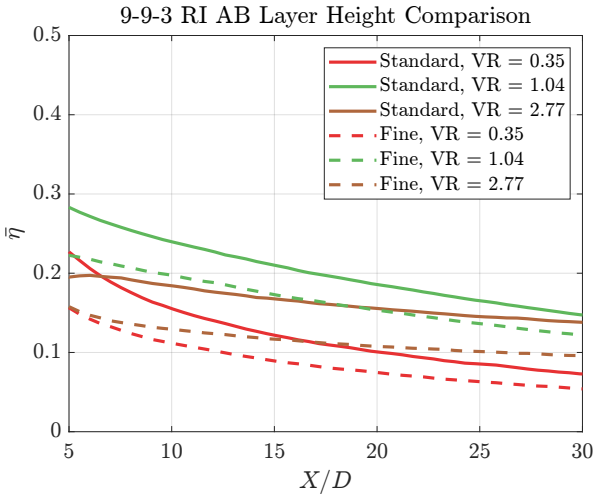

FIGURE 21: LATERALLY AVERAGED η FOR THE 9-9-3 RI USING STANDARD AND FINE BUILDS

Note that there is some hole to hole variation in the fine layer height case, notably for the topmost hole in the contour of the fine RI AB at $VR = 2.77$. Some artificial deformation in that hole as a result of the FDM build process may have occured. However, it can be observed that all holes have lower performance than the standard layer height case. This difference is interesting as in Fig. 10, roughness within the hole is evident in both the standard and fine RI AB hole. It is possible that by reducing the "frequency" of roughness, interaction with the flow changes. Larger valleys between ridges may contain recirculating vortices which prevent distortion of the flow. This same logic may be the reason the AD fine and standard layer height coupons perform similarly.

5. CONCLUSIONS

In this paper, two versions of a nominally 9-9-3 rounded inlet shaped film cooling hole were studied experimentally using both "as-designed" (AD) and "as-built" (AB) configurations. The two versions were a rounded inlet (RI) hole and modified rounded inlet and exit (RIE) hole intended to mitigate deformities caused by metal additive manufacturing (specifically DMLS). Although all test coupons were FDM printed, AD geometries were constructed to match design intent, while AB geometries included deformities and roughness features produced by DMLS at engine scale. These roughness features were captured directly from DMLS printed holes characterized for this study. Some of these geometries were also constructed using two different FDM layer height settings to evaluate the impact of layer height on print quality and performance. Following the construction of test coupons, experimental tests examined both adiabatic and overall cooling effectiveness using a new internal coolant co-flow experimental test section, which allows modular exchange of test surfaces and coupons. Major findings from the results of this study are summarized in the following list.

- As-built geometries printed with a layer height of 0.2 mm performed similarly to as-designed geometries. Current build processes with DMLS may be effective without degrading cooling performance.
- Hole diameter of as-built geometries tended to be oversized. As a result, it is imperative to consider differences in parameters such as P/D when evaluating as-built hole geometries vs those built as designed.
- Additional rounding in the RIE geometries does not appear to significantly improve the performance of the AB geometry printed using a layer height of 0.2 mm. While there is some reduction in deformities, these changes are not significant to the performance recorded in this study.
- Bore cooling in the hole for overall cooling effectiveness cases is significant, and should be considered when evaluating film cooling hole designs. The results of this study suggest that bore cooling is augmented for AB geometries vs AD geometries.
- Differences in FDM printed layer height did not have a significant impact on the performance the RI AD hole, but did have a significant impact on the performance of the RI AB

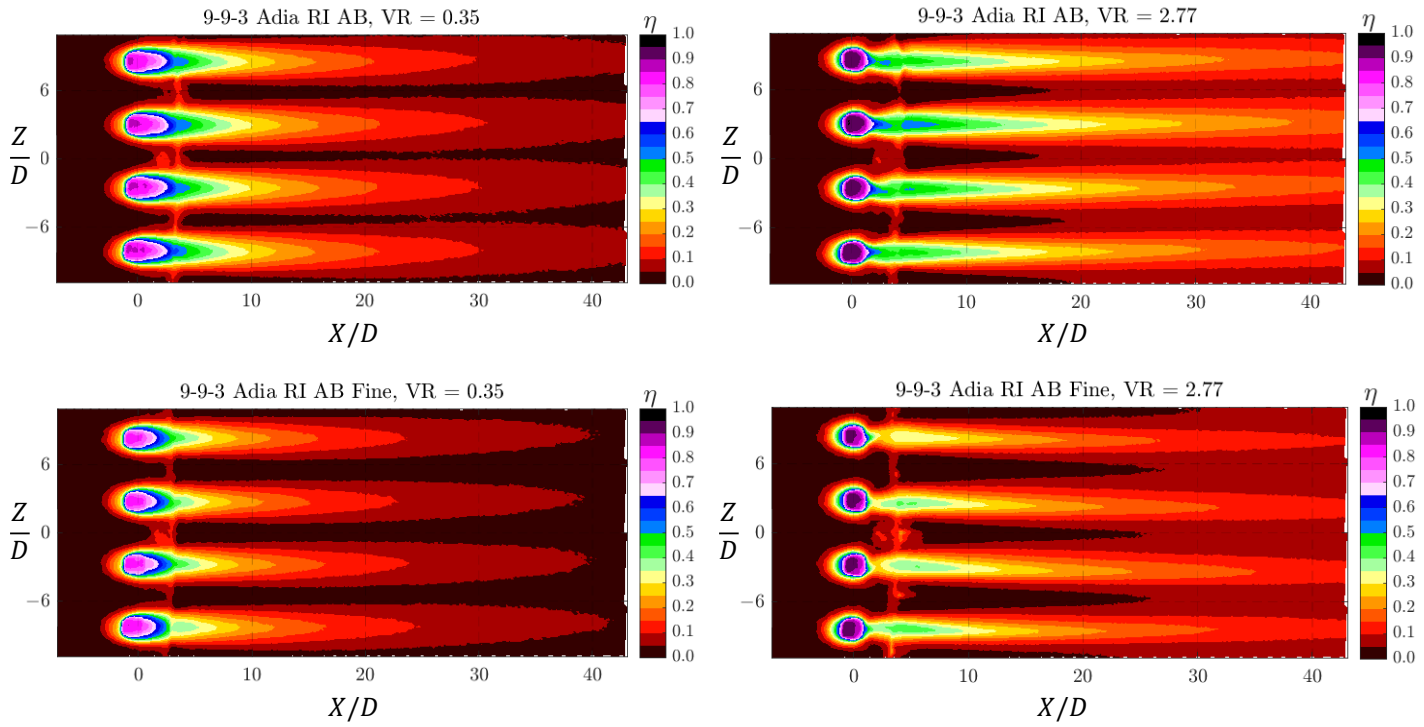

FIGURE 22: ADIABATIC EFFECTIVENESS CONTOURS FOR THE RI AB HOLE USING BOTH STANDARD AND FINE LAYER HEIGHTS

hole. Flow disruptions caused by smaller scale roughness may be significant.

Following this study, it can be said that DMLS holes manufactured with the hole aligned normal to the print bed may not have significant declines in performance due to manufacturing defects. Development of geometries using this build process should be continued and efforts to maintain that orientation for critical hole locations on blades/vanes should be implemented. While this study effectively examined large scale defects, it should be understood that limitations in capturing small scale surface roughness with FDM printers should be improved upon in future studies. Using other methods of resin based additive such as stereolithography (SLA) may improve print resolution and the ability to capture this roughness. Future studies should also improve experimental analysis by testing a range of VR_c.

6. ACKNOWLEDGMENTS

The authors would like to thank Pratt & Whitney and the U.S. Department of Energy - National Energy Technology Laboratory for sponsoring research presented in this paper. This paper is based upon work supported by the Department of Energy under Award Number DE-FE0025011. This report was prepared as an account of work sponsored by an agency of the United States Government. Neither the United States Government nor any agency thereof, nor any of their employees, makes any warranty, express or implied, or assumes any legal liability or responsibility for the accuracy, completeness, or usefulness of any information, apparatus, product, or process disclosed, or represents that its use would not infringe privately owned rights. Reference herein to any specific commercial product, process, or service by trade name, trademark, manufacturer, or otherwise does not necessarily constitute or imply its endorsement, recommendation, or favoring by the United States Government or any agency thereof. The views and opinions of authors expressed herein do not necessarily state or reflect those of the United States Government or any agency thereof. Furthermore, note that some color schemes presented in this paper are sourced from two online references. Color Brewer by Cynthia A. Brewer [27] and the Matlab function Linspecer created by Jonathan C. Lansey [28].

REFERENCES

[1] Reed, Roger C. *The superalloys: fundamentals and applications*. Cambridge University Press, Cambridge, UK ; New York (2006). OCLC: ocm65468245.

[2] Bogard, D. G. and Thole, K. A. "Gas Turbine Film Cooling." *Journal of Propulsion and Power* Vol. 22 No. 2 (2006): pp. 249–270. DOI 10.2514/1.18034.

[3] Schroeder, Robert P. and Thole, Karen A. "Adiabatic Effectiveness Measurements for a Baseline Shaped Film Cooling Hole." *Volume 5B: Heat Transfer*: p. V05BT13A036. 2014. American Society of Mechanical Engineers, Düsseldorf, Germany. DOI 10.1115/GT2014-25992.

[4] Gritsch, M., Schulz, A. and Wittig, S. "Adiabatic Wall Effectiveness Measurements of Film-Cooling Holes With Expanded Exits." *Volume 3: Heat Transfer; Electric Power; Industrial and Cogeneration*: p. V003T09A029.

1997. American Society of Mechanical Engineers, Orlando, Florida, USA. DOI 10.1115/97-GT-164.

[5] Gritsch, Michael, Schulz, Achmed and Wittig, Sigmar. "Effect of Internal Coolant Crossflow on the Effectiveness of Shaped Film-Cooling Holes." *Journal of Turbomachinery* Vol. 125 No. 3 (2003): pp. 547–554. DOI 10.1115/1.1580523.

[6] Stimpson, Curtis K., Snyder, Jacob C., Thole, Karen A. and Mongillo, Dominic. "Effectiveness Measurements of Additively Manufactured Film Cooling Holes." *Journal of Turbomachinery* Vol. 140 No. 1 (2018): p. 011009. DOI 10.1115/1.4038182.

[7] Stimpson, Curtis K., Snyder, Jacob C., Thole, Karen A. and Mongillo, Dominic. "Effects of Coolant Feed Direction on Additively Manufactured Film Cooling Holes." *Journal of Turbomachinery* Vol. 140 No. 11 (2018): p. 111001. DOI 10.1115/1.4041374.

[8] Jones, Fraser B., Fox, Dale W. and Bogard, David G. "Experimental and Computational Investigation of Shaped Film Cooling Holes Designed to Minimize Inlet Separation." 2020. American Society of Mechanical Engineers, London, England.

[9] Jones, Fraser B. III and Bogard, David G. "Parametric Optimization of Film Cooling Hole Geometry." *ASME Turbo Expo 2021: Power for Land, Sea, and Air*. 2021. DOI 10.1115/GT2021-59326.

[10] Vinton, Kyle R., Nahang-Toudeshki, Sara, Wright, Lesley M. and Carter, Andrew. "Full Coverage Film Cooling Performance for Combustor Cooling Manufactured Using DMLS." *Volume 5B: Heat Transfer*: p. V05BT17A005. 2016. American Society of Mechanical Engineers, Seoul, South Korea. DOI 10.1115/GT2016-56504.

[11] Dyson, Thomas E., McClintic, John W., Bogard, David G. and Bradshaw, Sean D. "Adiabatic and Overall Effectiveness for a Fully Cooled Turbine Vane." *Volume 3B: Heat Transfer*: p. V03BT13A037. 2013. American Society of Mechanical Engineers, San Antonio, Texas, USA. DOI 10.1115/GT2013-94928.

[12] Stimpson, Curtis K., Snyder, Jacob C., Thole, Karen A. and Mongillo, Dominic. "Roughness Effects on Flow and Heat Transfer for Additively Manufactured Channels." *Journal of Turbomachinery* Vol. 138 No. 5 (2016): p. 051008. DOI 10.1115/1.4032167.

[13] McClintic, John W., Anderson, Joshua B., Bogard, David G., Dyson, Thomas E. and Webster, Zachary D. "Effect of Internal Crossflow Velocity on Film Cooling Effectiveness—Part I: Axial Shaped Holes." *Journal of Turbomachinery* Vol. 140 No. 1 (2018): p. 011003. DOI 10.1115/1.4037997.

[14] Bunker, Ronald S. "Evolution of Turbine Cooling." *Volume 1: Aircraft Engine; Fans and Blowers; Marine; Honors and Awards*: p. V001T51A001. 2017. American Society of Mechanical Engineers, Charlotte, North Carolina, USA. DOI 10.1115/GT2017-63205.

[15] Bergman, T. L. and Incropera, Frank P. (eds.). *Fundamentals of heat and mass transfer*, 7th ed. Wiley, Hoboken, NJ (2011).

[16] Anderson, Joshua B., Boyd, Emily J. and Bogard, David G. "Experimental Investigation of Coolant-to-Mainstream Scaling Parameters With Cylindrical and Shaped Film Cooling Holes." *Volume 5B: Heat Transfer*: p. V05BT12A033. American Society of Mechanical Engineers. DOI 10.1115/GT2015-43072.

[17] Yoon, Christopher, Gutierrez, Daniel, Furgeson, Michael T. and Bogard, David G. "Evaluation of Adjoint Optimized Hole - Part II: Parameter Effects on Performance." *Proceedings of ASME Turbo Expo 2022*. American Society of Mechanical Engineers. DOI GT2022-82726.

[18] Snyder, Jacob C., Stimpson, Curtis K., Thole, Karen A. and Mongillo, Dominic. "Build Direction Effects on Additively Manufactured Channels." *Journal of Turbomachinery* Vol. 138 No. 5 (2016): p. 051006. DOI 10.1115/1.4032168.

[19] Reinhart. "Industrial CT and Precision." *Volume Graphics GmbH* .

[20] Veley, Emma M., Thole, Karen A., Furgeson, Michael T. and Bogard, David G. "Printability And Overall Cooling Performance Of Additively Manufactured Holes With Inlet And Exit Rounding." 2022. American Society of Mechanical Engineers, Rotterdam, The Netherlands.

[21] Wilkes, Ellen, Anderson, Joshua, McClintic, John and Bogard, David. "An Investigation of Turbine Film Cooling Effectiveness With Shaped Holes and Internal Cross-Flow With Varying Operational Parameters." *Volume 5C: Heat Transfer*: p. V05CT19A004. 2016. American Society of Mechanical Engineers, Seoul, South Korea. DOI 10.1115/GT2016-56162.

[22] Anderson, Joshua B., Wilkes, Ellen K., McClintic, John W. and Bogard, David G. "Effects of Freestream Mach Number, Reynolds Number, and Boundary Layer Thickness on Film Cooling Effectiveness of Shaped Holes." Vol. Volume 5C: Heat Transfer. DOI 10.1115/GT2016-56152.

[23] TCPoly. "Technial Datasheet: Ice9 Rigid." https://tcpoly.com/wp-content/uploads/2020/08/TDS_ice9_Rigid.pdf (2020). Online; accessed 1 September 2020.

[24] Figliola, R. S. and Beasley, Donald E. *Theory and design for mechanical measurements*, sixth edition ed. John Wiley & Sons, Hoboken (2015). OCLC: ocn897445548.

[25] Montgomery, Douglas C. and Runger, George C. *Applied statistics and probability for engineers*, 3rd ed. Wiley, New York (2003).

[26] Moffat, Robert J. "Describing the uncertainties in experimental results." *Experimental Thermal and Fluid Science* Vol. 1 No. 1 (1988): pp. 3–17. DOI 10.1016/0894-1777(88)90043-X.

[27] Brewer, Cynthia A. "ColorBrewer: Color Advice for Maps." (2013). Accessed 2021-10-18, URL https://colorbrewer2.org.

[28] Lansey, Jonathan C. "Beautiful and distinguishable line colors + colormap." (2015). Accessed 2021-10-18, URL https://www.mathworks.com/matlabcentral/fileexchange/42673-beautiful-and-distinguishable-line-colors-colormap.